.

Modified Titanium Surface with Nano Amorphous Calcium Phosphate@Chitosan Oligolactate as Ion Loading Platform with Multifunctional Properties for Potential Biomedical Application

Marijana R. Pantović Pavlović[1,2], Nenad L. Ignjatović[3], Senka Gudić[4], Ladislav Vrsalović[4], Katarina Đ. Božić[1,2], Marko E. Popović[1], Miroslav M. Pavlović[1,2,*]

[1]Department of Electrochemistry, Institute of Chemistry, Technology and Metallurgy, National Institute of the Republic of Serbia, University of Belgrade, 11000 Belgrade, Serbia
[2]Center of Excellence in Chemistry and Environmental Engineering—ICTM, University of Belgrade, 11000 Belgrade, Serbia
[3]Institute of Technical Science of the Serbian Academy of Sciences and Arts, 11000 Belgrade, Serbia
[4]Faculty of Chemistry and Technology, University of Split, 21000 Split, Croatia

Marijana R. Pantović Pavlović ORCID https://orcid.org/0000-0002-9507-3469
Nenad L. Ignjatović ORCID https://orcid.org/0000-0002-5749-094X
Senka Gudić ORCID https://orcid.org/0000-0001-5390-5215
Ladislav Vrsalović ORCID https://orcid.org/0000-0001-6111-5475
Katarina Đ. Božić ORCID https://orcid.org/0000-0002-6712-0221
Marko E. Popović ORCID https://orcid.org/0000-0003-0934-5550
Miroslav M. Pavlović ORCID https://orcid.org/0000-0003-3754-4143
*corresponding author e-mail: miroslav.pavlovic@ihtm.bg.ac.rs

Abstract
Titanium (Ti) is widely used in medical and dental implants. Calcium phosphate (CPs) coatings enhance Ti implants' osteoinductive properties, and additives further improve these coatings. Recently, a nano amorphous calcium phosphate (nACP) coating decorated with chitosane oligolactate (ChOL) and selenium (Se) showed immunomodulatory effects. This study investigates the surface morphology, composition, bioactivity, mechanical properties, and Se release mechanism of the nACP@ChOL-Se hybrid coating on Ti substrates. Amorphous calcium phosphate (ACP) was synthesized, and the nACP@ChOL-Se hybrid coating was deposited on Ti substrates using in situ anaphoretic deposition. Physico-chemical characterization was used to analyze the surface of the coating (scanning electron microscopy (SEM), X-ray diffraction (XRD) and Fourier Transform Infrared Spectroscopy (FTIR)). The distribution of Se within the coating was examined with energy dispersive X-ray spectroscopy (EDS). Bioactivity was evaluated in simulated body fluid (SBF), and adhesion was tested using a scratch test method. In vitro testing determined the release mechanism of Se. SEM images illustrated the surface morphology, while AFM provided a detailed analysis of surface roughness. XRD analysis revealed structural and phase composition, and EDS confirmed Se distribution within the coating. The coating exhibited bioactivity in SBF and showed good adhesion according to the scratch test. In vitro testing uncovered the release mechanism of Se from the coating. This study successfully characterized the surface morphology, composition, bioactivity, and Se release mechanism of the nACP@ChOL-Se hybrid coating on Ti substrates, offering insights for developing immunomodulatory coatings for medical and dental applications.

Keywords: hybrid coating; ion release; implants; bioactivity; nano calcium phosphate

Competing Interests
The authors declare no conflict of interest.

Acknowledgments
This work was supported by the Ministry of Science, Technological Development and Innovation of the Republic of Serbia (grant No. 451-03-47/2023-01/200026 and grant No. 451-03-66/2024-03/200175).

1. Introduction

Thus far, titanium (Ti) has been widely utilized as a material for creating diverse implants in the field of medicine and dentistry [1]. The addition of hydroxyapatite (HAp) coatings to titanium (Ti) substrates has proven to be highly effective in enhancing the osteoinductive properties of these implants, making them suitable for use in dentistry and medicine [2]. When jaw bone fixation is performed using HAp-coated Ti implants, a close bond is formed between the implant and the surrounding bone tissue, with no presence of other tissue in the interlayer [3]. The incorporation of nanostructured hydroxyapatite (nHAp) and similar calcium phosphates (CP) as coatings on Ti implants has further improved their properties, facilitating the earlier formation of new bone tissue [4]. Moreover, amorphous calcium phosphates (ACPs), which undergo a transformation into more stable structures like HAp, have demonstrated significant potential in the realm of reconstructive medicine [5].

Steel implants coated with HAp implanted in the tibia of sheep achieved a stronger interaction with the surrounding tissue compared to implants lacking an HAp coating [6]. Significant enhancement in the adhesion of surrounding bone tissue, thereby ensuring a more successful implant fixation, was also observed in implants made of titanium and coated with HAp [7]. Various titanium alloys based on Ti-6Al-4V, which are used in the fabrication of diverse medical devices today, have justified their coating with biocompatible and bioactive HAp for their more successful application in various medical contexts [8]. Hydroxyapatite-coated implants exhibited greater direct bone contact and more lamellar bone within the threads compared to titanium implants, regardless of their use in trabecular or cortical bone reconstruction [9,10].

In the quest to address implant-associated infections (IAIs), particularly in the case of titanium (Ti) implants, a range of strategies has been developed to effectively reduce IAIs [11,12]. One approach involves incorporating silver (Ag) into hydroxyapatite (HAp) coatings, resulting in the creation of a coating with antibacterial properties [13]. Furthermore, researchers have explored the antibacterial effects of Ti-coated HAp doped with various elements such as yttrium (Y), copper (Cu), and strontium (Sr) [14–16]. The presence of strontium (Sr), magnesium (Mg), and zinc (Zn) ions in HAp-based coatings has also demonstrated the ability to enhance their antibacterial properties [17].

In addition to ion doping in HAp, antibacterial properties can be achieved by employing hybrid coatings composed of HAp and polymers on titanium surfaces. Chitosan (Ch) and its derivatives, known for their excellent biocompatibility, non-toxicity, and favorable physical and chemical properties, possess remarkable antibacterial capabilities [18]. Micro-nanostructured HAp/chitosan (HAp/Ch) coatings on titanium substrates have shown the ability to inhibit the growth of various bacteria while simultaneously enhancing the coating's bioactivity potential [19]. Moreover, multifunctional coatings combining nano amorphous calcium phosphate (nACP) and chitosan oligosaccharide lactate (ChOL) have exhibited notable bioactive properties [20]. To ensure strong adhesion of nACP@ChOL coatings on titanium, a successful approach involves employing the simultaneous technique of anodization and anaphoretic electrodeposition [21].

Electrodeposition techniques have proven effective not only for depositing HAp/chitosan (HAp/Ch) coatings on titanium but also for incorporating antibiotics into these coatings [22]. Besides biocompatibility and mechanical properties, enhancing the bioactivity of HAp- or ACP-based coatings in conjunction with chitosan is crucial for their application in medicine and dentistry. The addition of cellulose acetate (CA) to nHAp/Ch-based coatings has demonstrated a significant improvement in bioactivity [23]. Additionally, the bioactivity of HAp/Ch-based coatings has been enhanced through the incorporation of carbon nanotubes and graphene during the electrodeposition process [22,24].

In addition to the previously discussed properties of nACP@ChOL and nHAp@ChOL coatings on titanium (Ti), which are crucial for their potential applications, the response of the body and organism after implantation represents a property of utmost importance. Generally, the introduction of a foreign object into the body of a mammal triggers complex biochemical processes that may lead to inflammation, infection, and other reactions [25]. Ongoing research in the field of HAp coatings on Ti substrates aims to develop coatings with properties that can reduce or completely inhibit the adverse response of the organism following implantation. In addition to essential properties such as biocompatibility, bioactivity, antibacterial properties, and corrosion stability, the latest generation of Ti coatings is also focused on their immunomodulatory properties. The design of biomaterials and coatings with anti-inflammatory characteristics presents a significant challenge for researchers today [26].

Studies have explored the incorporation of nonsteroidal anti-inflammatory drugs (NSAIDs) as part of HAp coatings on Ti substrates, and the results have shown no negative impact on the osseointegration of such implants while providing anti-inflammatory effects [27,28]. Furthermore, the addition of resveratrol to the HAp@Ch system has demonstrated simultaneous promotion of osteo-differentiation and significant anti-inflammatory effects during in vitro testing [29]. In our recent research, we have developed a nACP@ChOL-based coating decorated with selenium

(Se) on Ti using the anodization/anaphoretic electrodeposition process [30]. The deposited nACP@ChOL coatings exhibited a thickness of 240 ± 25 μm.
The focus of these studies was to investigate the immunomodulatory properties of the nACP@ChOL coatings decorated with Se on Ti in living systems, specifically in vivo. Selenium exhibits a range of desired properties such as antibacterial, antioxidant, anticancer, and immunomodulatory effects [31]. Particularly noteworthy are its pronounced antibacterial properties coupled with biocompatibility [32].
Due to its multifunctionality, low toxicity, high bioavailability, and high bioactivity, selenium is increasingly utilized not only as a dietary supplement but also as a medical therapeutic agent [33].The nACP@ChOL-Se (since the system is named this way at the beginning, it will be adopted throughout) coating has shown an increase in the Arg1 (arginase 1) ratio and M2/M1 (M2 macrophages/M1 macrophages) following implantation in a living organism, indicating its beneficial effect on the immune response. It is crucial to note that sodium selenite is highly soluble in water, yielding selenium as a byproduct [34].
The current study aims to investigate the surface morphology and specific characteristics of the nACP@ChOL-Se coating on titanium (Ti) substrates. During the electrodeposition process of nACP, its transformation into nanostructured hydroxyapatite (nHAp) takes place. X-ray structural analysis was employed to examine the coating's phases. The distribution of Se within the coating was analyzed using the suitable technique of Energy-Dispersive X-ray Spectroscopy (EDS). Furthermore, the potential bioactivity of the coating was evaluated in a simulated body fluid (SBF) environment. To assess the mechanical properties essential for potential applications and adhesion to the substrate surface, the Scratch test method was employed. Additionally, in vitro testing at a temperature of 37°C was conducted to determine the release mechanism of Se into the surrounding environment during potential applications.

2. Materials and Methods

Nano amorphous calcium phosphate (nACP) was synthesized by rapidly adding 150 mL of a 26.6% mass solution of $Ca(NO_3)_2$ x4H_2O (Sigma-Aldrich) in double-distilled water to 400 mL of an $(NH_4)_3PO_4$ solution. The later was prepared by combining 7 mL of H_3PO_4 (85%, Sigma-Aldrich), 165 mL of NH_4OH (28%, Sigma-Aldrich), and 228 mL of double-distilled H_2O. The resulting solution was continuously stirred at 100 rpm and 50°C for 60 minutes. The obtained fine gel was aged for 15 seconds before being collected, rinsed with water, and centrifuged at 4000 rpm in a Hettich Universal 320 centrifuge at 5°C for 1 hour. The resulting precipitate was freeze-dried at -30°C and a pressure of 0.37 bar for 1 hour, followed by a final drying step at -40°C and a pressure of 0.12 bar for 2 hours. The method was developed in the course of our earlier investigations [20,21,30,35–38].
For the *in situ* anaphoretic deposition processes of nACP@ChOL-Se hybrid multifunctional composite coatings on Ti substrates, 99.7% pure titanium plates (ThermoFisher) with dimensions of (20 × 10 × 0.89) mm were utilized. The titanium plates underwent precoating preparation which included sanding with silicon carbide (SiC) sandpaper with grit sizes of 600, 1000, 2000, and 3000, followed by polishing using alumina with grain sizes of 1, 0.3, and 0.05 μm (Buehler, IL, USA). Subsequently, all samples were washed and purified in 96% ethanol (Sigma Aldrich, Taufkirchen, Germany) using an ASONIC PRO 50 ultrasonic cleaner (ASonic, Ljubljana, Slovenia) with a power of 120 W and a frequency of 40 kHz for 30 minutes. To prevent spontaneous oxidation, the samples were stored in ethanol prior to deposition.
The nACP@ChOL-Se hybrid coatings on Ti substrates were obtained through in situ anaphoretic precipitation from an appropriate ethanolic suspension. To prepare the suspension, 273.5 mg of Na_2SeO_3 (equivalent to a total of 125 mg Se, Sigma Aldrich, Taufkirchen, Germany) was added to 50 mL of double-distilled water and stirred for 5 minutes until completely dissolved. Sodium selenite has been chosen as the source of selenium due to its high solubility in liquid media [39].
Next, 125 mg of chitosan oligosaccharide lactate (ChOL, Mw 5000, Sigma Aldrich, Taufkirchen, Germany) was added to the same solution, and the mixture was continuously stirred at 300 rpm overnight using a rotary magnetic stirrer. The total amount of selenium (125 mg) and a ChOL:Se mass ratio of 1:1 were selected as being continuation of the previous research [25]. After the ChOL had swelled and dissolved overnight, 50 mL of 96% ethanol and 1.000 g of ACP were added to the solution, followed by stirring at 300 rpm for another overnight. The pH was adjusted using 5 mL of 1 M NaOH to enhance the suspension's stability for subsequent anodization/anaphoretic deposition. The suspension was continuously mixed on a rotary magnetic stirrer at 300 rpm to ensure particle homogenization and maintain a stable suspension throughout the deposition process. The in situ anaphoretic deposition was performed using a custom-made two-electrode electrochemical cell, with the titanium plate (20 × 10 × 0.89) mm serving as the anode and a pair of 316 grade stainless steel plates (20 × 10 × 0.89) mm as the cathode, placed parallel to the anode at a distance of 10 mm. The nACP@ChOL-Se hybrid coatings on titanium were deposited at a constant voltage of 60 V for 1 minute, followed by air-drying for 24 hours at 25°C.

The surface morphology of the hybrid coatings was analyzed using field-emission scanning electron microscopy (Tescan Mira 3 XMU FEG-SEM). EDS analysis was conducted using a Jeol JSM 5800 SEM with a SiLi X-ray detector (Oxford Link Isis series 300, Abingdon, UK). The composite samples surfaces were sputter coated prior to SEM. Surface properties of the polymer composites were examined utilizing a contact mode atomic force microscope (AFM) known as "Nanoscope III," an AFM Multi-Mode Scanning Probe Microscope produced by "Digital Instruments" (Munich, Germany). The acquired microscopic data underwent analysis through the NanoScope Analysis software. The composite samples were subjected to X-ray diffraction (XRD) analysis for structural and phase evaluation. The measurements were carried out using a Philips PW 1050 powder diffractometer (Malvern Panalytical Ltd, Malvern, UK) at room temperature. Ni-filtered Cu Kα radiation (λ = 1.54178 Å) and a scintillation detector were used within the 2θ range of 3–82° with a scanning step size of 0.02°. The scanning rate was set at 5 seconds per step. Phase analyses were conducted using EVA V.9.0 software. To assess the adhesion of the coatings, the ASTM D 3359-02 Standard Test Methods for Measuring Adhesion by Tape, cross-cut tape test (B), was performed. The adhesion measurements were recorded using a camera equipped with a Leica 20 MP Ultra Wide Angle Lens and an aperture of f/2.2.

The concentration of selenium (total, in all oxidation states present in the coating and released to SBF solution) was measured using the inductively coupled plasma optical emission spectrometry (ICP-OES) analytical technique. SBF had the following ion concentrations: Na^+ 142.0 mM, K^+ 5.0 mM, Mg^{2+} 1.5 mM, Ca^{2+} 2.5 mM, Cl^- 148.8 mM, HCO^{3-} 4.2 mM, HPO_4^{2-} 1.0 mM, SO_4^{2-} 0.5mM [40,41]. ICP-OES measurements were performed on an iCAP 6500 Duo ICP instrument (Thermo Fisher Scientific, Cambridge, UK) with iTEVA operating software. The samples were introduced into the plasma by direct liquid aspiration. Calibration standard solutions in the appropriate concentration range (1-50000 µg/L) were prepared from a certified standard solution: Selenium, plasma standard solution, Specpure®, Se 1000 µg/ml (Alfa Aesar GmbH & Co KG, Germany). The correlation coefficient for selenium was >0.99. Selenium quantification was performed at the emission wavelength of Se I 196.090 nm. The concentration measurements were repeated three times (n=3). The relative standard deviation of the repeated measurements was RSD < 0.5%. For determination of total Se content in the hybrid coating, the coating was dissolved in aqua regia (HCl + HNO_3, 3:1 v/v) by boiling. The titanium plate remained intact and undissolved. After complete dissolution of the entire coating, the solution was quantitatively transferred to a volumetric flask with a capacity of 25 mL and diluted to the marked volume. The concentration of selenium in the resulting solution was measured using the ICP-OES analytical technique.

Michelson MB Series Bomen Fourier transform infrared spectroscope (FTIR) spectroscope (Hartmann Braun, Munich, Germany) was used to conduct FTIR analysis. The FTIR measurements were carried out in the wavenumber range of 400 to 4000 cm^{-1} with a spectral resolution of 0.5 cm^{-1}.

3. Results

3.1. Hybrid nACP@ChOL-Se coating characterization

To characterize the physical appearance and surface area of the synthesized hybrid nACP@ChOL-Se coatings on titanium substrates, SEM imaging was employed. Fig. 1 depicts the nACP@ChOL-Se hybrid coating prepared by in situ anodization/anaphoretic deposition process, which was performed for 1 minute, which is the same as in our previous research [30].

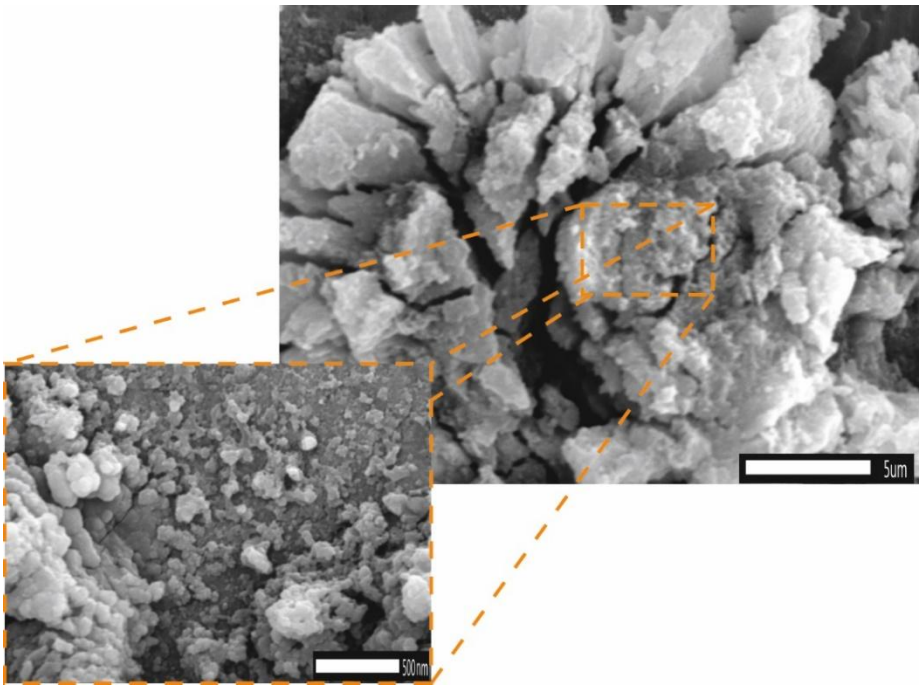

Fig. 1 SEM images of nACP@ChOL-Se hybrid coating on titanium substrate deposited by in situ anodization/anaphoretic deposition process at 60 V of the hybrid coating.

Figure 2 shows two -dimensional AFM pictures with surface morphology and linear roughness analysis of the nACP@ChOL-Se hybrid coating surface.

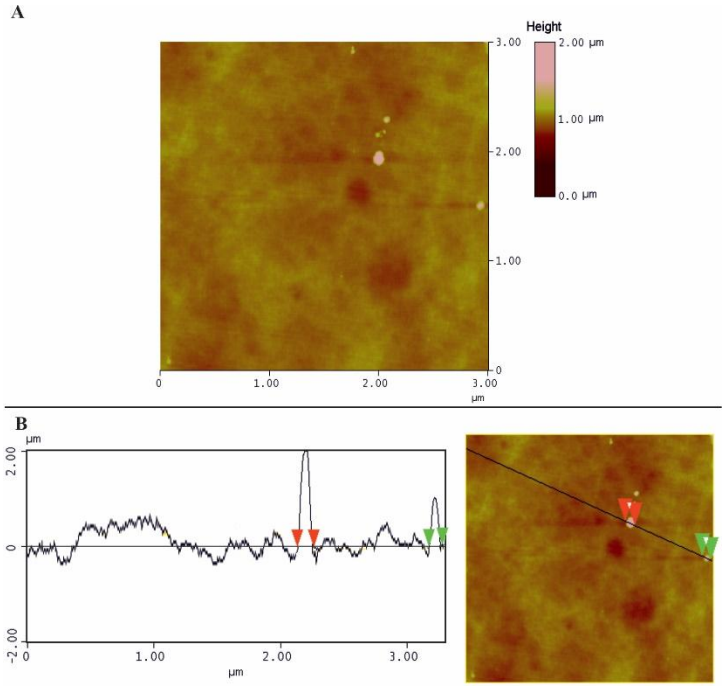

Fig. 2 Two-dimensional AFM image of the nACP@ChOL-Se hybrid coating surface with linear roughness analysis.

The EDS area analysis results, presented in Fig. 3 through EDS mapping, provided confirmation of the presence of building constituents, namely titanium (Ti), oxygen (O), calcium (Ca), phosphorus (P) and selenium (Se), in the nACP@ChOL-Se hybrid coating on titanium substrate.

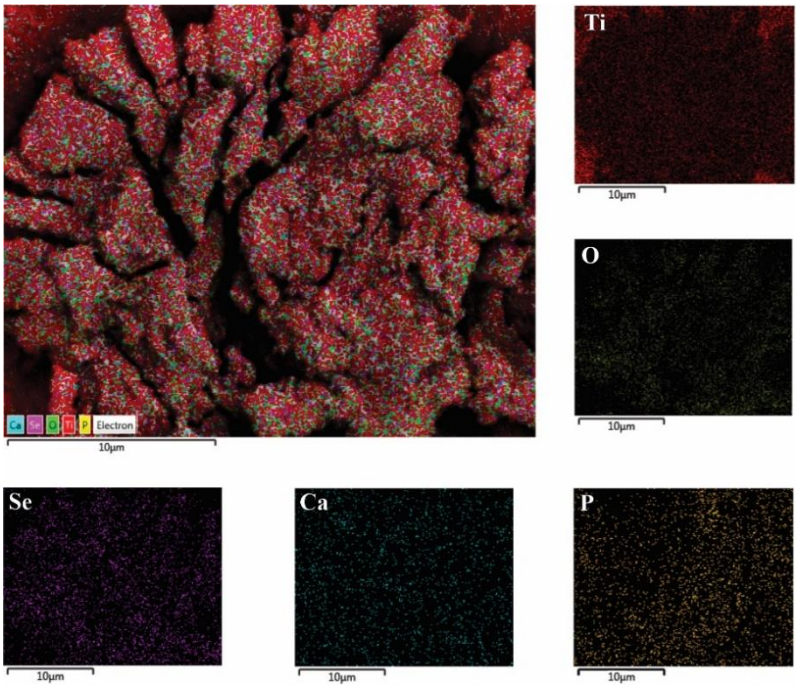

Fig. 3 EDS mapping of nACP@ChOL-Se hybrid coating on titanium substrate with all ions distribution and distribution of titanium (Ti), oxygen (O), selenium (Se), calcium (Ca) and phosphorus (P).

Fig. 4 displays the XRD diffraction pattern of nACP@ChOL-Se hybrid coating on the titanium substrate.

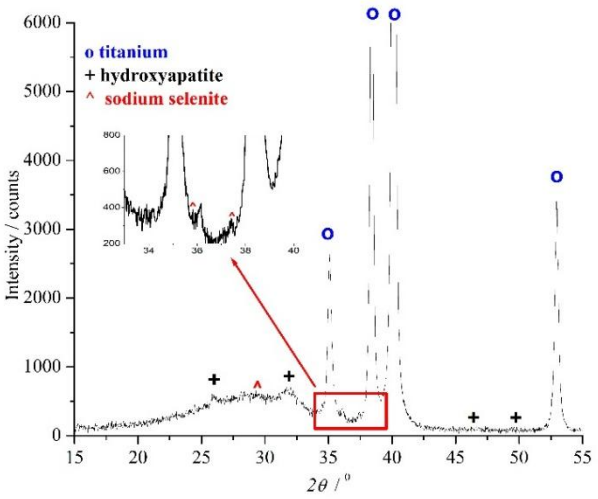

Fig. 4 XRD diffractogram of nACP@ChOL-Se hybrid coating on titanium substrate deposited by in situ anodization/anaphoretic deposition process at 60 V after 1 min of deposition with enlarged portion of the spectrum from 2Θ=32° to 40°.

The optical images of the nACP@ChOL-Se hybrid coating on titanium substrate before and after performing adhesion testing, quantified by adhesion test according to ASTM D 3359-02: Standard Test Methods for Measuring Adhesion by Tape; cross-cut tape test (B), are shown in Fig. 5.

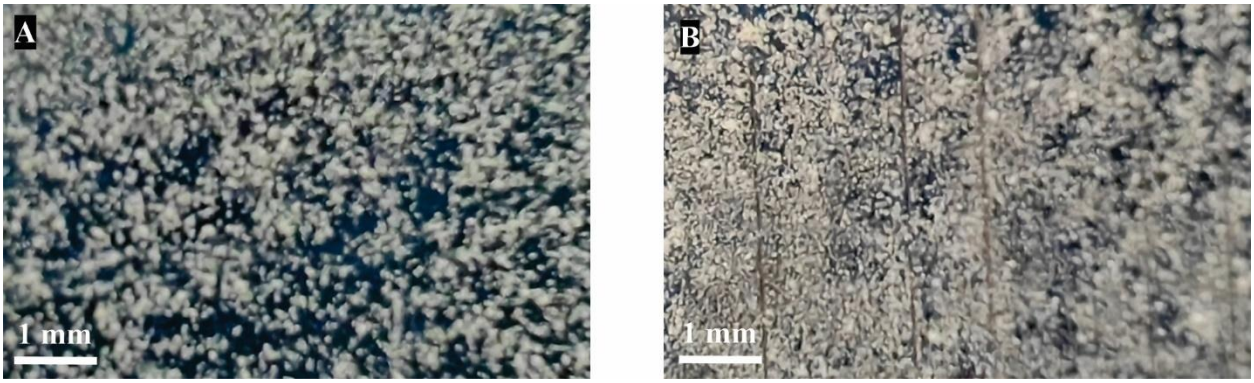

Fig. 5 Optical image of the nACP@ChOL-Se hybrid coating on titanium substrate obtained at 60 V (A) before and (B) after performing adhesion testing according to ASTM D 3359-02.

3.2. Bioactivity

Bioactivity encompasses a spectrum of intricate phenomena directly pertaining to absorption and surface activities influenced by various molecules [42]. In our investigations, we scrutinized bioactivity through the concept of the specific surface response within the material interphase-material environment, resulting in the formation of a new phase conducive to biological interactions [41].
To evaluate the bioactivity of the composite coatings, the nACP@ChOL-Se hybrid coatings on titanium substrate were subjected to immersion in SBF solution and analyzed at different time intervals. The surface morphologies of the hybrid composites after immersion in the SBF solution are presented in Fig. 6 (namely, Fig. 6A after 3 days of immersion and Fig 6B after 10 days of immersion).

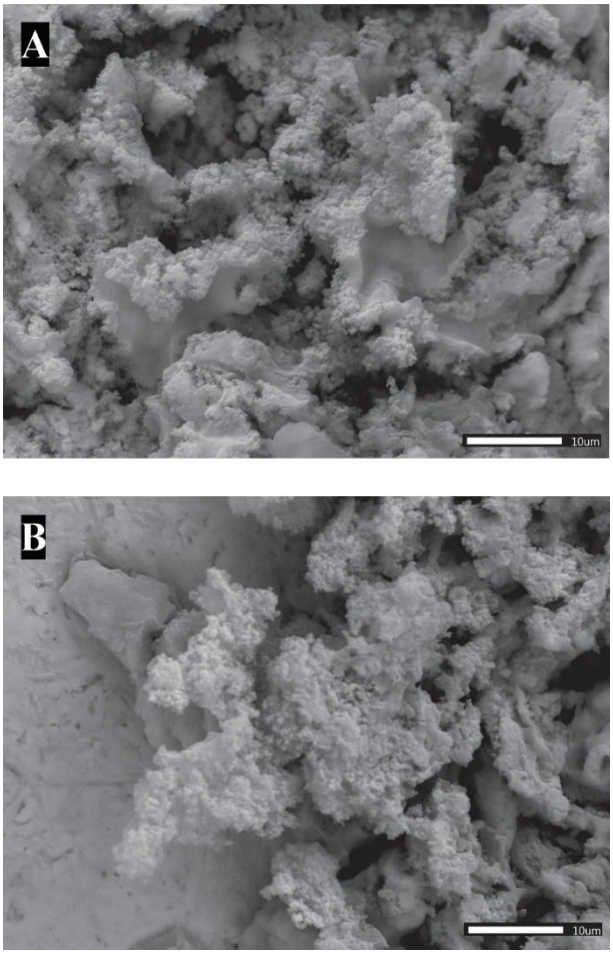

Fig. 6 (A) SEM micrograph of the nACP@ChOL-Se hybrid coatings on a titanium substrate after immersion in the SBF solution for 3 days. (B) SEM micrograph of the coatings after 10 days of immersion in the SBF solution.

Fig. 7 shows the EDS mapping analysis results of the nACP@ChOL-Se hybrid coatings after immersion in SBF for 10 days.

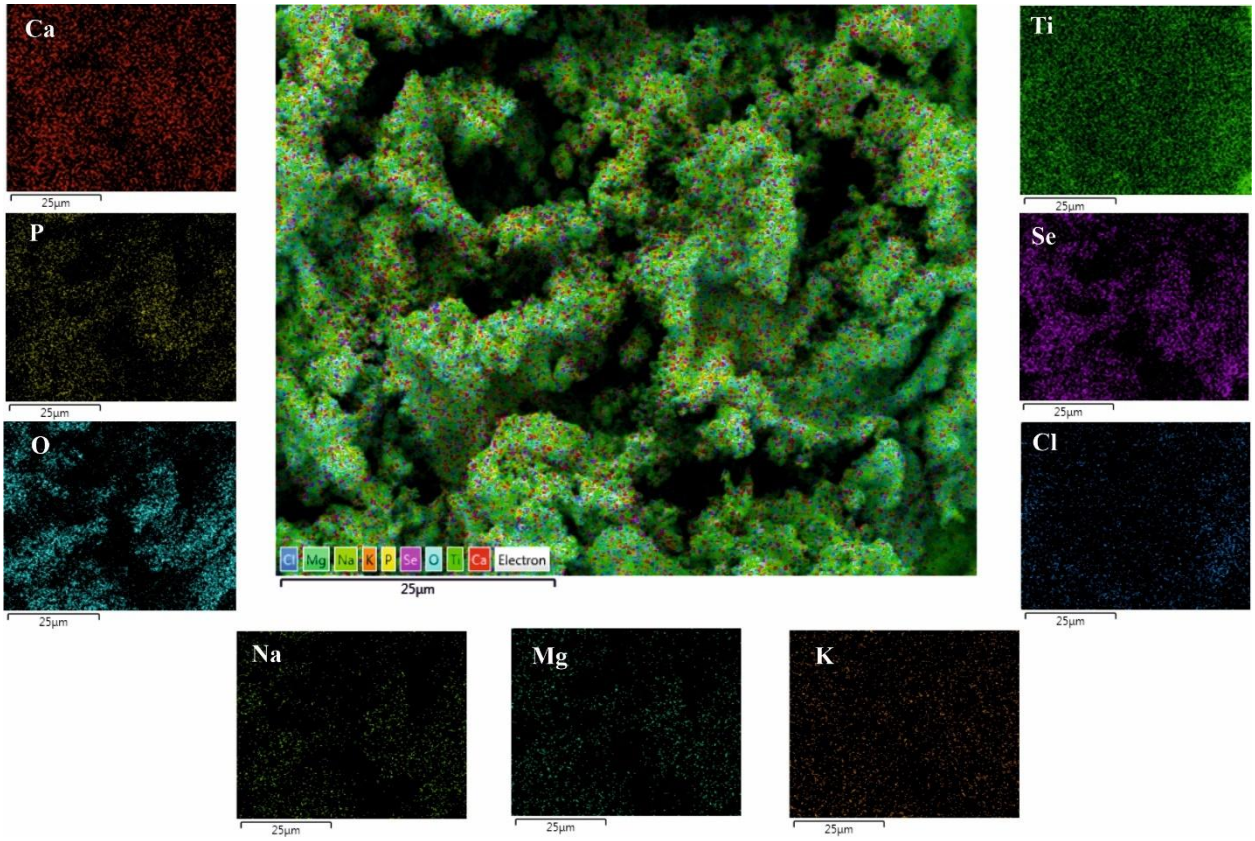

Fig. 6 EDS mapping of nACP@ChOL-Se hybrid coating on titanium substrate after immersion in SBF for 10 days with all ions distribution and distribution of titanium (Ti), oxygen (O), selenium (Se), calcium (Ca), phosphorus (P), Sodium (Na), magnesium (Mg), potassium (K) and chloride (Cl).

The FTIR spectra of the nACP@ChOL-Se hybrid coatings before and after 10 days immersion in SBF are presented in Fig. 8. The changes in the peaks' intensities, as well as appearances or disappearances of the peaks are labeled with numbers, which is discussed in the Discussion section.

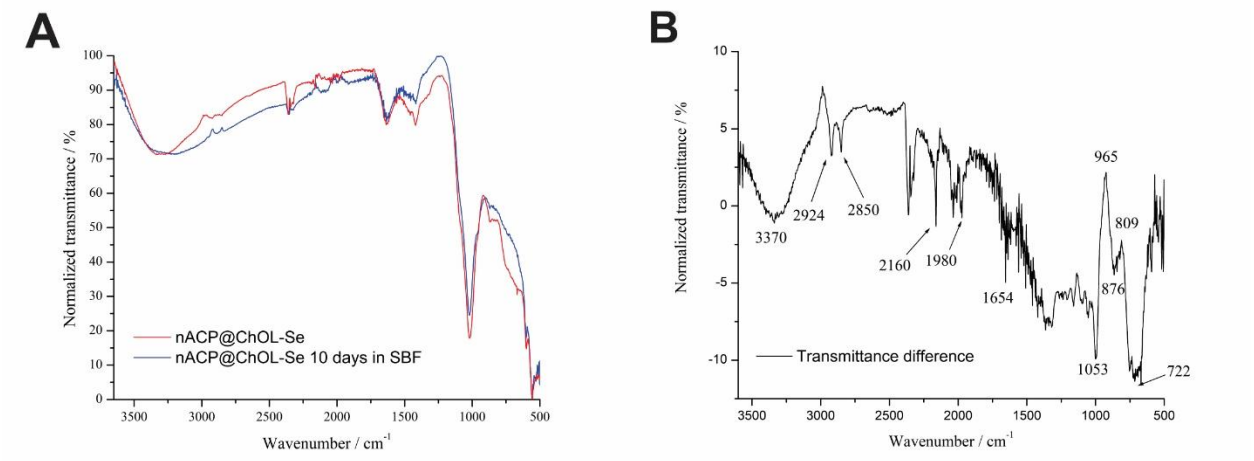

Fig. 8 (A) Normalized FTIR spectra of nACP@ChOL-Se hybrid coatings on titanium substrate before and after 10 days immersion in SBF, (B) Difference between normalized transmittances of nACP@ChOL-Se hybrid coatings on titanium substrate after and before 10 days immersion in SBF.

3.3. Ion release study

The results of our previous research [30] have unequivocally confirmed that the nACP@ChOL-Se multifunctional hybrid composite coating on a titanium substrate has the immunomodulatory and anti-inflammatory effect compared to the pure grade 2 titanium implants. However, it was of the utmost importance to investigate the Se-release mechanism in vitro. The results of the investigation of selenium release in SBF medium is shown in Fig. 8.

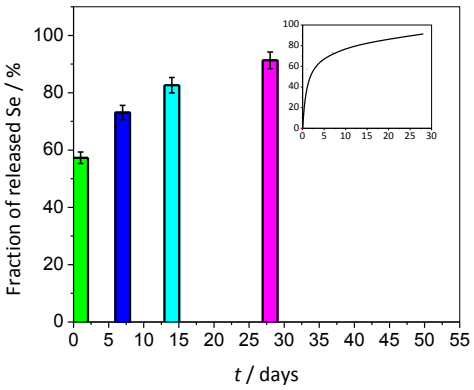

Fig. 8 (A) Cumulative curve of the release of selenium in SBF medium at 37°C over the investigated time period.

4. Discussion

From the Fig. 1 it can be observed that the deposited coating has a rose flower-like structure, which is attributed to the in situ process mechanism, as already explained in our previous research [30]. Due to the potentiostatic conditions during deposition and presence of more conductive species in the suspension used for deposition of nACP@ChOL-Se hybrid coatings, higher values of current densities are obtained, being up to 30 mA/cm^2. As explained, the hydrogen gas evolution results in the formation of pits, holes, and vacancies, creating the rose flower-like structure which can be observed in Fig. 1. Nevertheless, the hybrid coating is completely covering the substrate and this coating consists of agglomerated nanoparticles, and this can be observed on the enlarged part of the structure from Fig. 1. It can be seen that the the entire structure is composed of agglomerates of nano particles of ACP, ChOL and selenite, which is proven by EDS measurements. The presence of these agglomerates contributes to the formation of a rough surface, which is crucial for promoting beneficial osteoconductivity. In previous research [30], it was shown that macroscale RMS value was 2.153 µm. The AFM depiction of the surface morphology of the ACP/ChOL/Se hybrid coating, as depicted in Figure 2A, substantiates the aforementioned statement. As illustrated in Figure 2A, the examined surface (with a scan area of 3×3 µm) appears relatively smooth. The linear roughness profile, depicted in Figure 2B, reveals a root mean square roughness (RMS) value of 1.364 µm and a surface roughness of 13.8 µm. The results are comparative to linear surface roughness measurements which were carried out in much greater scale (over 1 mm) and done in previous researches. They indicate the condensation and agglomeration of the coating, with starting particles smaller than 100 nm [30]. The presence of these agglomerates contributes to the formation of a rough surface, crucial for fostering beneficial osteoconductivity.

The homogeneity of the deposited hybrid coating's structure can be observed from EDS measurements presented in Fig. 3. All the constituents, namely amorphous calcium phosphate (ACP) represented by calcium (Ca) and phosphorus (P) and selenium additive (Se), are evenly distributed across the titanium (Ti) substrate. Oxygen (O) presence is due to the polymer, oxidized titanium in the form of titanium dioxide, and the selenium salt used with the process of anodization/anaphoretic deposition process.

The XRD pattern of the nACP@ChOL-Se hybrid coating is presented in Fig. 4. The XRD analysis indicates that hybrid coating exhibits characteristic wide amorphous diffraction maximum with maximum around 2θ=30°, suggesting that the main component of the coatings is ACP. Additionally, XRD pattern of nACP@ChOL-Se hybrid coating shows distinct diffraction peaks at 2θ=25.85° and 31.6° which correspond to (002) and (211) reflections of the HAp crystal lattice (JCPDS standard XRD card No. 86–1199). Furthermore, small peak at 2θ=46.6° and 49.6° correspond to (222) and (213) reflections of the HAp crystal lattice [43]. Reflection peak at 2θ=29.3°, as well as diffraction peaks at 2θ=35.8° and 37.4° from the enlarged section of the XRD diffractogram correspond to (213),

(303) and (411) reflections of the body centered tetragonal crystal lattice of sodium selenide (JCPDS standard XRD card No. 86-1846) [44]. Due to smaller quantity of the used precursors, the former peak intensities are smaller. The XRD results confirm the transformation of amorphous ACP to crystalline HAp, ant that single-step in situ electrophoretic deposition occurs, with depositing all the species from the starting precursor solution.

The adhesion of composite coatings plays a crucial role in determining the potential biomedical applications of any composite material in the future. In order to evaluate the adhesion of nACP@ChOL-Se hybrid coatings on Ti substrate, a comprehensive adhesion test was conducted according to ASTM D 3359-02 Standard Test Methods for Measuring Adhesion by Tape, cross-cut tape test (B), given its significance for the potential medical applications of this composite material. Fig. 5 shows the optical images of the nACP@ChOL-Se hybrid coating on titanium substrate after performing the adhesion test. After conducting a thorough assessment of the adhesion of the hybrid composite coating according to the ASTM D3359-02 standard, the adhesion level was determined to be 5, on a scale where 5 represents the highest adhesion (no delamination or flaking) and 0 represents the lowest adhesion (more than 65% of the coating delaminated). There is no influence of ion loading on adhesion of the hybrid coating, since the adhesion is not affected when compared to our previous work [21]. The enduring stability of coatings under the rigors of potential exploitation underscores a critical aspect of material performance. The prerequisite for this sustained stability lies in the establishment of a coating with robust adherence to the substrate. Specifically, the assessment of coatings founded on calcium phosphate compounds constitutes a multifaceted and intricate realm of investigation. The intricacy of this evaluation demands a specialized focus within research endeavors, ensuring a comprehensive understanding of the coating's behavior and longevity. Rigorous investigations are thus essential to yield results that are not only insightful but also valid, contributing significantly to the advancement of materials science and engineering in practical applications [45,46].

The in vitro bioactivity of a substrate refers to its ability to form an apatite layer when exposed to biologically similar fluids. To evaluate the bioactivity of nACP@ChOL-Se hybrid coatings on titanium substrate, they were immersed in SBF solution for up to 10 days and analyzed at different time intervals. The SEM results from Fig. 6 clearly demonstrate the bioactivity of nACP@ChOL-Se hybrid coating following immersion in SBF. A complete coverage of the sample surface by a new apatite layer is evident. As it can be seen in Fig. 6A, even after 3 days new HAp-like layer is formed in the form of granulated agglomerates with particle sizes of few tens to 50 nm in diameter. After 10 days (Fig. 6B), it can be seen that the surface of the hybrid composite is completely covered with the newly formed apatite layer, and there is continuation of apatite growth in the form of spread across the composite surface, with continued growth of apatite in the form of granulated globular agglomerates. The formation of HAp from SBF serves as preliminary evidence for the composite-coated Ti's potential for in vivo bone bonding capability. The bone-like HAp layer formed on the implant surface after immersion in SBF is believed to support cell cascading and protein signaling, leading to the formation of new bone tissue [47]. It has been observed that this bone-like HAp layer possesses excellent osteoconductivity and exhibits a strong affinity for living bone cells [48]. Moreover, it facilitates the proliferation of osteoblast cells, promoting the generation of new bone tissue. Therefore, the development of an HAp layer along the implant material's surface is a crucial requirement for the successful osseointegration between the implant and the surrounding living bone tissue.

EDS mapping analysis results of the hybrid composites after 10 days of immersion in SBF, shown in Fig. 7, confirm the bioactivity of the tested samples. Besides all the constituents (calcium (Ca), phosphorus (P), oxygen (O), selenium (Se) and titanium (Ti)), the presence of sodium (Na), magnesium (Mg), potassium (K) and chloride (Cl) was observed. Besides Ca, P and O, the later were incorporated in the top layer during immersion of samples in SBF, which is one of the proofs for bioactivity.

FTIR examination was performed on the hybrid samples before and after 10 days of immersion in SBF, and the results are shown in Fig. 8. As the new apatite layer is formed, there are some changes in the bands and intensities. The presence of distinct band difference at 2924 cm^{-1} and 2850 cm^{-1} (Fig. 8B) corresponds to C-H stretch vibration of the methylene groups from ChOL, showing that, due to apatite layer being grown on top, there is disappearance of these characteristic ChOL bands. [49–52]. The characteristics FTIR bands that appear, and are visible as the most distinguishable bands in transmittance difference graph (Fig. 8B) at 965 cm^{-1} and 1053 cm^{-1} correspond, namely to ν1 symmetric stretching vibration of P–O band of PO_4^{3-} ion and ν3 asymmetric stretching mode of vibration of P–O bands of PO_4 tetrahedra [53–55]. The spectral data at the wave number values of 3370 cm^{-1}, 1980 cm^{-1} and1654 cm^{-1} suggest the structural and adsorbed H_2O, and, directly, O–H presence in the prepared hybrid composite coating [53–55]. Also, appearance of band at 876 cm^{-1} in transmittance difference graph (Fig. 8B) suggests the presence of carbonate ion in the prepared hybrid composite coating, i.e. the obtained apatite is a B-type carbonated apatite, and the part of the PO_4 (B-type) groups in the apatitic structure was replaced by CO_3^{2-} groups [53,55]. Diminishing bands in the transmittance difference graph at 809 cm^{-1} and 722 cm^{-1} correspond to the SeO_3^{2-} ion being covered with apatite layer, and Se being released to the medium. Besides the HAp layer formation on top of the

nACP@ChOL-Se hybrid coating during immersion in SBF, there is release of selenium ions to the medium. Hence the quantity of selenium is lowered. Therefore, the bands that correspond to sodium selenite is diminishing [49–51]. The FTIR results undoubtedly confirm the bioactivity of nACP@ChOL-Se hybrid coating on titanium substrate. During a 28-day timeframe, the hybrid composite system underwent an observation of selenium release. Fig. 9 depicts the dynamics of selenium release in a simulated body fluid (SBF) solution at 37°C under static conditions. The commonly used Peppas model [56] was employed to determine the release parameters by fitting the curve depicted in Fig. 8.

$$M_t/M_\infty = kt^n, \quad (1)$$

The Peppas model, represented by Equation 1, was utilized to mathematically describe the kinetics of drug delivery. In this equation, M_t/M_∞(%) represents the cumulative release proportionate to the release constants k (h^{-1}) the diffusional exponent n which characterizes the release mechanism [56]. The Peppas model belongs to the category of empirical or semi-empirical mathematical models [57] that are employed to calculate the diffusional exponent n, indicating the transport mechanism.

The fitting results indicate that the release mechanism of selenium from the investigated nanocomposite biomaterials under static conditions conforms to an anomalous transport mechanism (upper part of the Fig. 9). This type of release mechanism, referred to in literature as non-Fickian transport, is observed. Notably, an increase in selenium content tends to shift the release mechanism towards Fickian diffusion. Non-Fickian transport is typically observed when a drug is released from thin polymer layers [58,59]. The dominant phenomenon in cases of non-Fickian transport is the presence of high elastic stress in the polymer, associated with a nonlinear relaxation time [60]. The underlying premise posits that within liquid environments, ChOL experiences degradation processes, concomitant with the liberation of selenium. The intricate phenomenon of polymer degradation, specifically based on chitosan, in aqueous solutions encompasses the comprehensive breakdown of the polymer matrix into constituent units. This breakdown results in the formation of smaller fractions, notably including monomers such as D-glucosamine and N-acetyl-glucosamine. The elucidation of this intricate degradation pathway is pivotal in understanding the fate of ChOL in liquid media, providing valuable insights into the dynamics of polymer behavior and the consequent release of selenium species. Such detailed investigations contribute to advancing our knowledge in the realm of polymer science, with implications for various applications, including controlled drug release and biomedical engineering [61–63].

Fig. 9 illustrates the progression of selenium release over the course of 28 days. Following the first day, the highest release rate occurs between the first and seventh day (15.8%), followed by the period between 7 and 14 days (9.5%), and finally between days 14 and 28 (8.7%). The initial higher release rate is likely attributed to the substantial amount of selenium present in the starting composite due to the synthesis procedure. Accelerated release can be observed in all systems during the first 10 days, during which 78% of the total selenium amount is released in the system.

After the implantation of a foreign body into the organism, an immediate occurrence of the foreign body reaction (FBR) takes place within the implant-tissue interface. Acute inflammatory processes manifest within the first 24 hours following the implantation of the foreign body into the organism [64,65]. The initial or early immune response of the organism to the foreign body/implant is also crucial for the expression of proinflammatory cytokines that direct the immune response of the organism [66]. For these reasons, we aimed to steer the early immune response of the organism within the first 24 hours after implantation towards the suppression of inflammatory reactions by delivering a larger quantity of selenium, which is present in the coating. Through optimization of the deposition process, variation of Se content within the coating, and substitution of ChOL with different bioresorbable polymers in the coating, we believe it would be feasible to comprehensively design both the quantity and delivery time of Se from the coating, without limitations.

Since Se is present in the ChOL matrix, the assumption is that in liquid media, there is degradation/breakdown of ChOL accompanied by the release of Se. The degradation of Ch-based polymers in aqueous solutions refers to the process wherein the polymer substance breaks down into smaller fractions, such as monomers (D-glucosamine, N-acetyl-glucosamine) [61,62]

5. Conclusions

The nACP@ChOL-Se hybrid coatings on titanium substrates displayed a distinctive rose flower-like structure attributed to an *in situ* process. Despite the unique morphology caused by hydrogen gas evolution during deposition, the coating maintained complete coverage and consisted of agglomerated nanoparticles, confirmed by SEM/EDS analyses. EDS measurements affirmed homogeneity, and XRD analysis identified a primarily nano amorphous calcium phosphate (nACP) composition transforming into hydroxyapatite (HAp) during the deposition process.

Adhesion testing rated the coatings at 5, unaffected by ion loading. In simulated body fluid (SBF), the coatings showed bioactivity, forming an apatite layer that could promote potential osseointegration. EDS mapping confirmed additional elements' incorporation during immersion. Release dynamics fitting the Peppas model indicated anomalous transport, transitioning to Fickian diffusion with increased selenium content. Initial higher release rates decreased over time. Overall, the coatings exhibit favorable characteristics for biomedical applications, showing promise for orthopedic implants and medical devices. Further studies are needed to assess long-term stability, cytocompatibility, and corrosion performance.
In recent years, a new generation of HAp coatings has emerged on various titanium implants, facilitating the release of various drugs, thus rendering such coatings multifunctional. These coatings enable controlled delivery of antibiotics [11,67,68], hormones [69], vitamins [70], etc. Our research is directed towards designing coatings that release metalloids (Se) and, in addition to their biocompatible, osteoconductive, and antibacterial properties, could enhance corrosion resistance, which is also crucial in potential medical applications and is the subject of our future investigations.

Author Contributions
Marijana R. Pantović Pavlović – conceptualization, methodology, validation, investigation, data curation, writing—original draft preparation, writing—review and editing, supervision
Nenad L. Ignjatović – conceptualization, methodology, formal analysis, resources, writing—review and editing, supervision, funding acquisition
Senka Gudić – investigation, writing—original draft preparation, writing—review and editing
Ladislav Vrsalović – investigation, resources, writing—review and editing, funding acquisition
Katarina Đ. Božić – investigation, visualization
Marko E. Popović – validation, investigation
Miroslav M. Pavlović – methodology, validation, formal analysis, resources, data curation, writing—original draft preparation, writing—review and editing, visualization, supervision, funding acquisition

Acknowledgements
This work was supported by the Ministry of Science, Technological Development and Innovation of the Republic of Serbia (grant No. 451-03-47/2023-01/200026 and grant No. 451-03-47/2023-01/200175).

Data Availability Statement
Data are available on request from the corresponding authors due to privacy restrictions.

Competing Interests
The authors declare no conflict of interest.

References
1. D. F. Williams, *Titanium for Medical Applications BT - Titanium in Medicine: Material Science, Surface Science, Engineering, Biological Responses and Medical Applications* (Springer Berlin Heidelberg, Berlin, Heidelberg, 2001), pp. 13–24.
2. U. Ripamonti, L. C. Roden, L. F. Renton, Biomaterials 33, 3813 (2012) 10.1016/j.biomaterials.2012.01.050.
3. G. L. de Lange, K. Donath, Biomaterials 10, 121 (1989) https://doi.org/10.1016/0142-9612(89)90044-6.
4. L. Meirelles, A. Arvidsson, M. Andersson, P. Kjellin, T. Albrektsson, A. Wennerberg, J. Biomed. Mater. Res. Part A 87A, 299 (2008) https://doi.org/10.1002/jbm.a.31744.
5. S. V Dorozhkin, Biomater. Sci. 9, 7748 (2021) 10.1039/D1BM01239H.
6. A. Moroni, S. Toksvig-Larsen, M. C. Maltarello, L. Orienti, S. Stea, S. Giannini, JBJS 80, (1998).
7. A. E. Porter, P. Taak, L. W. Hobbs, M. J. Coathup, G. W. Blunn, M. Spector, Biomaterials 25, 5199 (2004) https://doi.org/10.1016/j.biomaterials.2003.12.018.
8. Gunawarman, J. Affi, A. Sutanto, D. M. Putri, D. Juliadmi, N. F. Nuswantoro, H. Fajri, D. H. Tjong, M. Manjas, IOP Conf. Ser. Mater. Sci. Eng. 1062, 12031 (2021) 10.1088/1757-899X/1062/1/012031.
9. G. M. J. Vidigal, L. C. Argenta Aragones, A. J. Campos, M. Groisman, Implant Dent. 8, (1999).
10. T. Hayakawa, M. Yoshinari, H. Kiba, H. Yamamoto, K. Nemoto, J. A. Jansen, Biomaterials 23, 1025 (2002) 10.1016/S0142-9612(01)00214-9.
11. S. Akshaya, P. K. Rowlo, A. Dukle, A. J. Nathanael, Antibiotics 11, 1719 (2022) 10.3390/antibiotics11121719.
12. X. Chen, J. Zhou, Y. Qian, L. Zhao, Mater. Today Bio 19, 100586 (2023) https://doi.org/10.1016/j.mtbio.2023.100586.

13. N. A. Trujillo, R. Floreani, H. Ma, J. D. Bryers, J. D. Williams, K. C. Popat, Mater. Sci. Eng. C 32, 2135 (2012) https://doi.org/10.1016/j.msec.2012.05.012.
14. K. Zhang, B. Zhang, C. Huang, S. Gao, B. Li, R. Cao, J. Cheng, R. Li, Z. Yu, X. Xie, J. Mech. Behav. Biomed. Mater. 100, 103363 (2019) https://doi.org/10.1016/j.jmbbm.2019.07.021.
15. Q. Li, S. Song, J. Li, J. Yang, R. Zhang, M. Niinomi, T. Nakano, Mater. Trans. 63, 1072 (2022) 10.2320/matertrans.MT-M2021245.
16. Z. Geng, R. Wang, X. Zhuo, Z. Li, Y. Huang, L. Ma, Z. Cui, S. Zhu, Y. Liang, Y. Liu, H. Bao, X. Li, Q. Huo, Z. Liu, X. Yang, Mater. Sci. Eng. C 71, 852 (2017) https://doi.org/10.1016/j.msec.2016.10.079.
17. Y.-C. Liu, Y.-T. Lee, T.-C. Huang, G.-S. Lin, Y.-W. Chen, B.-S. Lee, K.-L. Tung, ACS Appl. Bio Mater. 4, 2523 (2021) 10.1021/acsabm.0c01535.
18. J. Li, S. Zhuang, Eur. Polym. J. 138, 109984 (2020) 10.1016/j.eurpolymj.2020.109984.
19. B. Li, X. Xia, M. Guo, Y. Jiang, Y. Li, Z. Zhang, S. Liu, H. Li, C. Liang, H. Wang, Sci. Rep. 9, 14052 (2019) 10.1038/s41598-019-49941-0.
20. M. R. Pantović Pavlović, B. P. Stanojević, M. M. Pavlović, M. D. Mihailović, J. S. Stevanović, V. V Panić, N. L. Ignjatović, ACS Biomater. Sci. Eng. 7, 3088 (2021) 10.1021/acsbiomaterials.1c00035.
21. M. R. Pantović Pavlović, M. M. Pavlović, S. Eraković, J. S. Stevanović, V. V. Panić, N. Ignjatović, Mater. Lett. 261, 127121 (2020) 10.1016/j.matlet.2019.127121.
22. M. Stevanović, M. Djošić, A. Janković, V. Kojić, J. Stojanović, S. Grujić, I. M. Bujagić, K. Y. Rhee, V. Mišković-Stanković, J. Mater. Res. Technol. 15, 4461 (2021) https://doi.org/10.1016/j.jmrt.2021.10.072.
23. Z. Zhong, J. Qin, J. Ma, Mater. Sci. Eng. C 49, 251 (2015) https://doi.org/10.1016/j.msec.2015.01.020.
24. P. C. Rath, B. P. Singh, L. Besra, S. Bhattacharjee, J. Am. Ceram. Soc. 95, 2725 (2012) https://doi.org/10.1111/j.1551-2916.2012.05195.x.
25. Y. Chandorkar, R. K, B. Basu, ACS Biomater. Sci. Eng. 5, 19 (2019) 10.1021/acsbiomaterials.8b00252.
26. E. Lebaudy, S. Fournel, P. Lavalle, N. E. Vrana, V. Gribova, Adv. Healthc. Mater. 10, 2001373 (2021) https://doi.org/10.1002/adhm.202001373.
27. V. E. Toy, S. Dundar, A. Bozoglan, J. Oral Biol. Craniofacial Res. 10, 333 (2020) https://doi.org/10.1016/j.jobcr.2020.06.006.
28. A. Salduz, F. Dikici, Ö. I. Kılıçoğlu, H. I. Balcı, T. Akgul, M. Kürkçü, C. Kurtoğlu, R. Tözün, J. Orthop. Surg. 25, 2309499016684410 (2017) 10.1177/2309499016684410.
29. L. Li, M. Yu, Y. Li, Q. Li, H. Yang, M. Zheng, Y. Han, D. Lu, S. Lu, L. Gui, Bioact. Mater. 6, 1255 (2021) https://doi.org/10.1016/j.bioactmat.2020.10.018.
30. M. R. Pantović Pavlović, N. L. Ignjatović, V. V Panić, I. I. Mirkov, J. B. Kulaš, A. L. Malešević, M. M. Pavlović, J. Funct. Biomater. 14, 227 (2023) 10.3390/jfb14040227.
31. A.-R. A. Nassar, A. M. Eid, H. M. Atta, W. S. El Naghy, A. Fouda, Sci. Rep. 13, 9054 (2023) 10.1038/s41598-023-35360-9.
32. F. Martínez-Esquivias, J. M. Guzmán-Flores, A. Pérez-Larios, N. González Silva, J. S. Becerra-Ruiz, J. Nanosci. Nanotechnol. 21, (2021).
33. D. Chen, H. Lu, Y. Ma, Y. Huang, T. Zhang, S. Fan, W. Lin, Y. Huang, H. Jin, Y. Ruan, J.-F. Xu, J. Pi, Front. Nutr. 10, (2023).
34. R. Sinha, T. K. Said, D. Medina, Cancer Lett. 107, 277 (1996) https://doi.org/10.1016/0304-3835(96)04373-X.
35. M. Pantović Pavlović, M. M. Pavlović, J. Kovačina, B. Stanojević, J. Stevanović, V. Panić, N. Ignjatović, J. Serbian Chem. Soc. (2021) 10.2298/JSC210211024P.
36. M. Pantovic-Pavlovic, M. Pavlovic, S. Erakovic, T. Barudzija, J. Stevanovic, N. Ignjatovic, V. Panic, M. R. Pantović Pavlović, M. M. Pavlović, S. Eraković, T. Barudžija, J. S. Stevanović, N. Ignjatović, V. V Panić, J. Serbian Chem. Soc. 84, 1305 (2019) 10.2298/JSC190730105P.
37. M. R. Pantović Pavlović, S. G. Eraković, M. M. Pavlović, J. S. Stevanović, V. V. Panić, N. L. Ignjatović, Surf. Coatings Technol. 358, 688 (2019) 10.1016/j.surfcoat.2018.12.003.
38. M. R. Pantović Pavlović, M. M. Pavlović, *In Situ Synthesis and Characterization of Anaphoretic Multifunctional Coatings on Titanium with Advanced Properties*, 1st ed. (Nova Science publishers, New York, NY, 2022), pp. 53–95.
39. M. Kousha, S. Yeganeh, A. Keramat Amirkolaie, Food Sci. Biotechnol. 26, 1013 (2017) 10.1007/s10068-017-0142-y.
40. T. Kokubo, H. Kushitani, S. Sakka, T. Kitsugi, T. Yamamuro, J. Biomed. Mater. Res. 24, 721 (1990) 10.1002/jbm.820240607.
41. F. Baino, S. Yamaguchi, Biomimetics 5, (2020) 10.3390/biomimetics5040057.
42. A. A. Mariod, H. E. Tahir, *Chapter 2 - Biological Activities, Definition, Types and Measurements* (Academic

Press, 2022), pp. 17–28.
43. R. Kotian, P. P. Rao, P. Madhyastha, Eur. J. Dent. 11, 438 (2017) 10.4103/ejd.ejd_100_17.
44. S. R. Youngren, R. Mulik, B. Jun, P. R. Hoffmann, K. R. Morris, M. B. Chougule, AAPS PharmSciTech 14, 1012 (2013) 10.1208/s12249-013-9988-3.
45. J. Schubert, M. Chanana, Curr. Med. Chem. 25, 4553 (2018) http://dx.doi.org/10.2174/0929867325666180601101859.
46. S. R. Paital, N. B. Dahotre, Mater. Sci. Eng. R Reports 66, 1 (2009) https://doi.org/10.1016/j.mser.2009.05.001.
47. T. Kokubo, H. M. Kim, M. Kawashita, T. Nakamura, J. Mater. Sci. Mater. Med. 15, 99 (2004) 10.1023/B:JMSM.0000011809.36275.0c.
48. A. M. Kumar, B. Suresh, S. Das, I. B. Obot, A. Y. Adesina, S. Ramakrishna, Carbohydr. Polym. 173, 121 (2017) https://doi.org/10.1016/j.carbpol.2017.05.083.
49. B. A. Jerri Al-Bakhsh, F. Shafiei, A. Hashemian, K. Shekofteh, B. Bolhari, M. Behroozibakhsh, Bioact. Mater. 4, 322 (2019) 10.1016/j.bioactmat.2019.10.004.
50. C. Combes, S. Cazalbou, C. Rey, Minerals 6, (2016) 10.3390/min6020034.
51. C. Rey, C. Combes, C. Drouet, H. Sfihi, A. Barroug, Mater. Sci. Eng. C 27, 198 (2007) https://doi.org/10.1016/j.msec.2006.05.015.
52. N. Akartasse, K. Azzaoui, E. Mejdoubi, L. L. Elansari, B. Hammouti, M. Siaj, S. Jodeh, G. Hanbali, R. Hamed, L. Rhazi, Polymers (Basel). 14, (2022) 10.3390/polym14204265.
53. S. Mondal, A. Mondal, N. Mandal, B. Mondal, S. S. Mukhopadhyay, A. Dey, S. Singh, Bioprocess Biosyst. Eng. 37, 1233 (2014) 10.1007/s00449-013-1095-z.
54. R. N. Panda, M. F. Hsieh, R. J. Chung, T. S. Chin, J. Phys. Chem. Solids 64, 193 (2003) https://doi.org/10.1016/S0022-3697(02)00257-3.
55. M. H. Fathi, A. Hanifi, V. Mortazavi, J. Mater. Process. Technol. 202, 536 (2008) https://doi.org/10.1016/j.jmatprotec.2007.10.004.
56. P. L. Ritger, N. A. Peppas, J. Control. Release 5, 23 (1987) https://doi.org/10.1016/0168-3659(87)90034-4.
57. J. Siepmann, F. Siepmann, Int. J. Pharm. 364, 328 (2008) https://doi.org/10.1016/j.ijpharm.2008.09.004.
58. M. F. Saettone, P. Chetoni, L. M. Bianchi, B. Giannaccini, U. Conte, M. E. Sangalli, Int. J. Pharm. 126, 79 (1995) https://doi.org/10.1016/0378-5173(95)04096-X.
59. A. Hasimi, A. Stavropoulou, K. G. Papadokostaki, M. Sanopoulou, Eur. Polym. J. 44, 4098 (2008) https://doi.org/10.1016/j.eurpolymj.2008.09.011.
60. D. A. Edwards, J. Polym. Sci. Part B Polym. Phys. 34, 981 (1996) https://doi.org/10.1002/(SICI)1099-0488(19960415)34:5<981::AID-POLB16>3.0.CO;2-7.
61. T. Kean, M. Thanou, Adv. Drug Deliv. Rev. 62, 3 (2010) https://doi.org/10.1016/j.addr.2009.09.004.
62. K. Piekarska, M. Sikora, M. Owczarek, J. Jóźwik-Pruska, M. Wiśniewska-Wrona, Polymers (Basel). 15, 793 (2023) 10.3390/polym15040793.
63. V. Miskovic-Stankovic, T. M. Atanackovic, Fractal Fract. 7, 518 (2023) 10.3390/fractalfract7070518.
64. L. Tang, J. W. Eaton, Mol. Med. 5, 351 (1999) 10.1007/BF03402124.
65. A. Carnicer-Lombarte, S.-T. Chen, G. G. Malliaras, D. G. Barone, Front. Bioeng. Biotechnol. 9, (2021).
66. N. Söhling, M. Ondreka, K. Kontradowitz, T. Reichel, I. Marzi, D. Henrich, Materials (Basel). 15, (2022) 10.3390/ma15062195.
67. M. Stigter, J. Bezemer, K. De Groot, P. Layrolle, J. Control. Release 99, 127 (2004) 10.1016/j.jconrel.2004.06.011.
68. Z. Liao, J. Li, Y. Su, F. Miao, X. Zhang, Y. Gu, J. Du, R. Hang, Y. Wei, W. Chen, D. Huang, Front. Mater. Sci. 17, 230628 (2023) 10.1007/s11706-023-0628-x.
69. Z.-S. Tao, W.-S. Zhou, Z. Qiang, K. Tu, Z.-L. Huang, H.-M. Xu, T. Sun, Y.-X. Lv, W. Cui, L. Yang, J. Biomater. Appl. 30, 952 (2015) 10.1177/0885328215610898.
70. N. Sarkar, S. Bose, ACS Appl. Mater. Interfaces 12, 13644 (2020) 10.1021/acsami.9b22474.